200
1-16-78

MASTER

HA. 1751

UCRL-52339

DETECTION AND MEASUREMENT OF POST-ROSENBLUTH CONVECTIVE INSTABILITY IN MFTF WITH A HYBRID CO_2 LASER-HETERODYNE DIAGNOSTIC SYSTEM

A. L. Peratt

October 5, 1977

Prepared for U.S. Energy Research & Development Administration under contract No. W-7405-Eng-48

Printed in the United States of America
Available from
National Technical Information Service
U.S. Department of Commerce
5285 Port Royal Road
Springfield, VA 22161
Price: Printed Copy $; Microfiche $3.00

Page Range	Domestic Price	Page Range	Domestic Price
001-025	$ 4.00	326-350	$12.00
026-050	4.50	351-375	12.50
051-075	5.25	376-400	13.00
076-100	6.00	401-425	13.25
101-125	6.50	426-450	14.00
126-150	7.25	451-475	14.50
151-175	8.00	476-500	15.00
176-200	9.00	501-525	15.25
201-225	9.25	526-550	15.50
226-250	9.50	551-575	16.25
251-275	10.75	576-600	16.50
276-300	11.00	601-up	[1]
301-325	*11.75*		

[1] Add $3.50 for each additional 100 page increment from 601 pages up.

Distribution Category
UC-21

LAWRENCE LIVERMORE LABORATORY
University of California/Livermore, California/94550

UCRL-52339

DETECTION AND MEASUREMENT OF POST-ROSENBLUTH CONVECTIVE INSTABILITY IN MFTF WITH A HYBRID CO_2 LASER–HETERODYNE DIAGNOSTIC SYSTEM

A. L. Peratt

MS date: October 5, 1977

CONTENTS

DETECTION AND MEASUREMENT OF POST-ROSENBLUTH CONVECTIVE INSTABILITY IN MFTF WITH A HYBRID CO_2 LASER–HETERODYNE DIAGNOSTIC SYSTEM

ABSTRACT

To measure and classify the Post-Rosenbluth convective loss-cone instability in MFTF, we propose to use a CO_2 laser consisting of a TEA-pulsed section and a low pressure CW section, together with a light mixing receiver. Calculations show that this system offers sufficient power and sensitivity to detect instability throughout the range from strong coherent light scattering to weak incoherent scattering when the instability is eliminated.

INTRODUCTION

The identification and elimination of microinstabilities which limit confinement times is a significant problem common to all magnetic confinement experiments. When these instabilities possess wavelengths in the range of a few microns to a few millimeters, 10.6 μm laser light may be used as a nonperturbing diagnostic probe. In Tokamak heating experiments, the ion-acoustic wave decay instability described by submillimeter wavelengths, can occur [1], while in large open-ended mirror machines, convective instabilities [2] are expected to occur with wavelengths between 0.1 mm and a few millimeters. The ion acoustic wave decay instability occurs at frequencies of tens to hundreds of megahertz, while the convective instability is expected at frequencies below the ion plasma frequency $\omega < \omega_{pi}$.

In the CO_2 laser diagnostics systems operating within the ten micrometer portion of the spectrum, the considerations of frequency, wavelength and instability/fluctuation amplitude are coupled with the availability of an efficient source and the need for mechanical tolerances that are within the capability of modern optical systems. In particular, an infrared wavelength makes possible the use of heterodyne detection, which would be impractical in the visible wavelengths.

Heterodyne detection of CO_2 light has been successfully used to measure and classify electron cyclotron harmonic waves [3] and to study the current-driven ion-acoustic instability. [4] In addition to measuring the Bragg scattered power from coherent waves or instabilities, the CO_2-heterodyne probe may also be used to investigate collective effects of thermal fluctuations in the incoherent spectrum. This is due to the fact that, in the forward scattering of infrared light, the effective probing wavelength is greater than the Debye length in fusion plasmas. Thus, distinct features in the spectral density, not seen at visible laser wavelengths, are resolvable within the infrared wavelengths. Progress along these lines have been made by Goldston et. al. on the Adiabatic Toroidal Compressor experiment, [5] and by Masters and Rye [6] who reported the first measurement of the ion-acoustic feature in high density plasma.

In all the above mentioned experiments, continuous or repeatedly pulsed laser light was used in conjunction with time-averaging receiving equipment. In a transient plasma, or a plasma whose microinstability or wave of interest is transitory in nature, time-averaging techniques cannot be employed. Instead, the laser-detector system must have sufficient power and sensitivity to detect within the time frame of the event to be recorded.

In a heterodyne receiver setup, the frequency content of the scattered and local-oscillator beams must be sufficiently pure so that the signal can be distinguished from interference due to frequency beating between higher-order longitudinal and transverse laser cavity modes. The hybrid laser offers a solution to this problem, since a single cavity contains both a high-pressure (large energy) pulsed section and a low-pressure (small energy), single-line selecting section.[7] Peratt, Watterson, and Derfler have detected and measured ion-acoustic waves on a 3-μsec time scale using pulse average powers of less than half a megawatt from such a system[3].

Hence, a hybrid CO_2-heterodyne detection scheme is well suited to investigate both instabilities and thermal fluctuations in plasma. Coherent scattering will yield information about energy transport and plasma containment, while incoherent scattering may be used to ascertain basic plasma parameters, including ion and electron temperatures and density.

Section 2 of this report describes the basic features of the source-detection diagnostics system. Section 3 describes the CO_2 laser characteristics and control. Section 4 discusses the details of photomixing and signal detection over the sensitive surface of a mercury cadmium telluride (HgCdTe) antenna/detector. System alignment and calibration suggestions for externally excited acoustic waves are given in Section 5. Sections 6 and 7 deal with the Post-Rosenbluth (P-R) instability and thermal fluctuation scattering, respectively, where signal-to-noise ratio estimates are calculated for available laser powers and heterodyne receiver sensitivities.

SYSTEM DESCRIPTION

The proposed system consists of a CO_2 infrared laser source and a light mixing receiver, consisting of focusing optics and a mercury cadmium telluride detector (Fig. 1). If the system is operated in the nontunable or "homodyne mode," the source laser may also be used as the receiver "local oscillator." Here the investigatable bandwidth (~1 GHz) is determined by the response time of the detector. For "heterodyne mode" operation, where the complete-thermal fluctuation spectrum (70 GHz for a forward scattered observation angle θ_s = 11 mrad) may be investigated, a separate CO_2 local oscillator is required.

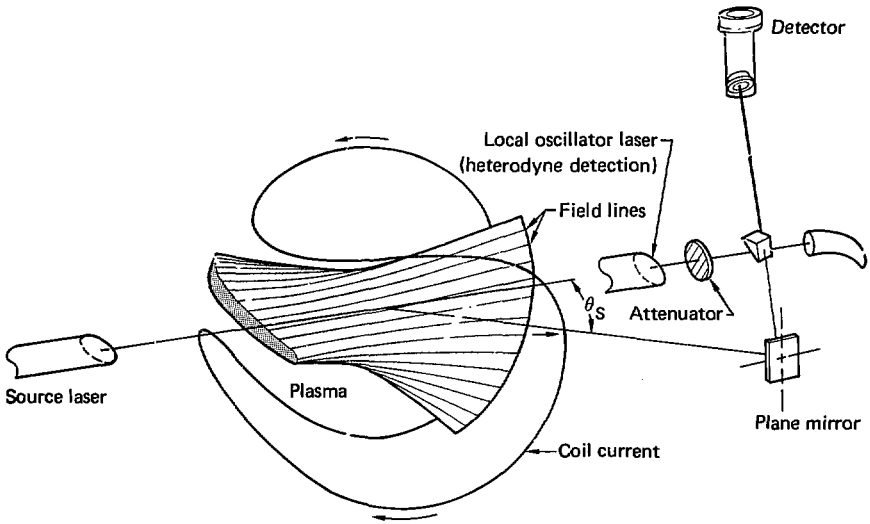

Fig. 1. Basic geometry of CO_2-heterodyne diagnostics system for MFTF plasma.

Since the scattering cross section of an electron is extremely small, we ideally require a laser with as high a power output as possible which will not perturb the plasma and which produces a single frequency output.

Hybrid CO_2 Laser System

High power continuous wave systems require high speed gas flow through the discharge region so that the temperature rise of the gas, which will be destructive of gain if it is too large, will be held to acceptable levels. The hardware necessary to sustain such flows is generally massive, expensive, and time-consuming to maintain. Usually transversely excited atmospheric (TEA)-pulsed lasers can only run for a few tens of microseconds at most before sparks between electrodes terminate operation.

TEA-pulsed lasers offer the power required when scattering results from the thermal fluctuation background or from instabilities whose coherence length is short (superthermal scattering). Typically, these lasers offer good temporal resolution since pulse lengths of 50 nsec to 20 μsec are obtainable.[9] In large part, the quick termination of the normal corona glow is due to the very high power level that is usual for such a system. Operation can be extended for microseconds only by lowering the power density.

An important consideration in the use of an atmospheric laser is its large collisional gainwidth (approximately 5 GHZ at atmospheric pressure). Hence, the growth and oscillation of a number of cavity longitudinal modes, spaced typically 30-60 MHz apart, is possible. Such oscillation is undesirable in a light-mixing scheme. Conversely, the low energy capability of a low-pressure laser has a gainwidth of 40-60 MHz, causing a large rejection ratio between some dominant longitudinal mode and its neighbor. Additionally, the low pressure section may be conveniently excited continuously for purposes of alignment and non-transient signal averaging. Therefore, by hybridizing a TEA section with a low-pressure section, high-peak pulse power operation can be attained at a single frequency (Fig. 2). Operation in three distinct modes is possible:

1. Low power continuous wave
2. Medium power repetition pulsed
3. High power pulsed.

Power levels currently associated with the above modes, respectively, are:

1. 10-100 W
2. 150 W pulse average power, 300 pps
3. 1 MW peak pulse power, ~1 μsec.

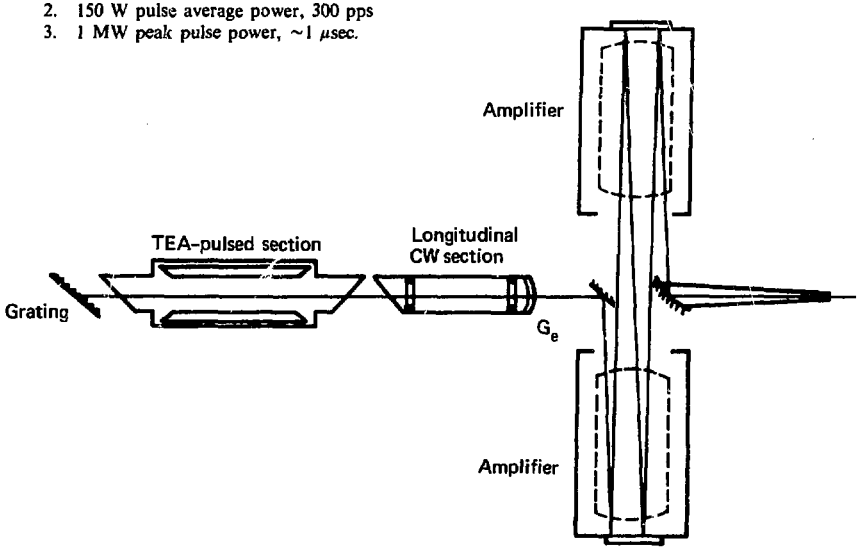

Fig. 2. Hybrid laser-amplifier system.

In the pulsed mode of operation, additional amplification providing a 4% cm^{-1} gain is depicted in Fig. 2. For a 0.5 J input, this amplification yields a 4 J output. In addition to the modes described above, a Q-switched, high repetition rate laser may be used. Typical parameters for such a system include 1.5 KW pulses with a duration of 0.1 μsec at a repetition rate of 400 pps. It should be mentioned that the above modes pertain to stable resonator operation. However, unstable resonator operation deserves further investigation. [10,11]

Focusing of the laser energy onto the plasma region of interest, as well as the observation at forward angles, is to be carried out with spherical mirrors and Ge or ZnSe windows.

Light-Mixing Receiver

The configuration for a heterodyne receiver in the infrared [12] is shown in Fig. 3. Its operation is made possible by the nonlinear response at the photodetector to the incident total radiation electric field. [13] Two electromagnetic waves of different frequencies (ω_s and ω_i) mix at the photodevice and produce an electrical signal with the difference frequency ($\omega_s - \omega_i$). When one of these beams is made strong enough (the "local" oscillator), the sensitivity of the process is considerably increased over the straight detection case because of the high conversion gain between power at the input and difference frequencies. In addition to this high conversion gain, the heterodyne detector exhibits both strong directivity and frequency selectivity. It is the frequency selectivity of the coherent detection process that permits the noise bandwidth to be reduced to a very small value. The heterodyne detector is linear only insofar as the detector output power is proportional to the input signal radiation power.

At optical and infrared frequencies, the heterodyne detector acts as both an antenna and a receiver, and has an integrated effective aperture limited by approximately λ_i^2. [14] Careful alignment between the LO and signal beams is necessary to maintain a constant phase across the surface of the photodetector. [15,16] Consequently, heterodyne detection is most useful for detecting weak signals that are coherent with a locally produced source.

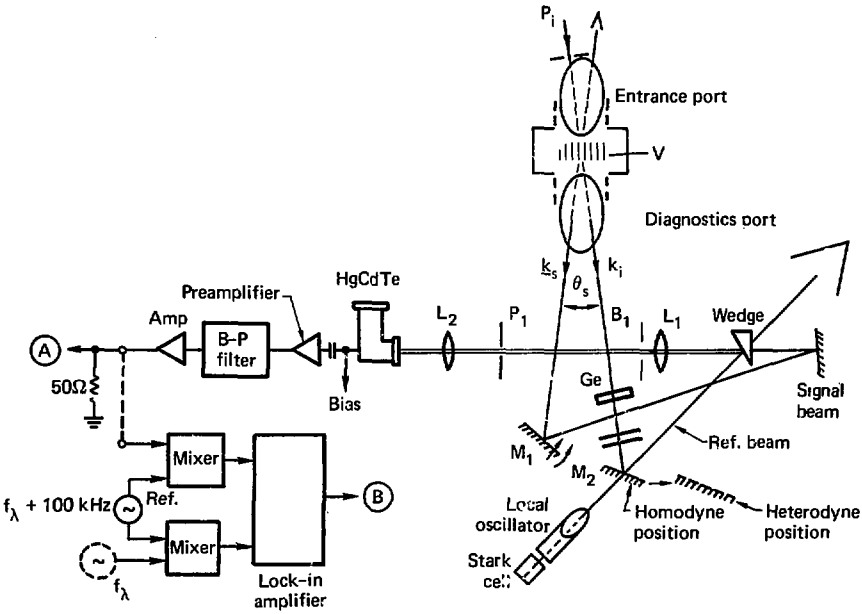

Fig. 3. Homodyne-heterodyne light-mixing receiver system.

When the signal and the local oscillator both derive from the same source (homodyne detection), the heterodyne signal can provide information about the velocity of the scatterer through the Doppler shift. Here the frequency response of the photodiode is

$$\omega_s - \omega_i = 2\pi (\nu_{Tj} + f_\lambda - \nu_{Tj}) = \omega_\lambda \tag{1}$$

where f_λ is the frequency of a signal with wavelength λ, and ν_{Tj} is some j^{th} transistional laser frequency. Where the local oscillator and signal beams arise from different, but frequency-locked, lasers (heterodyne detection), the response of the photodiode is

$$\omega_s - \omega_i = 2\pi (\nu_{Tj} + f_\lambda - \nu_{Tj+n}) = 2\pi (f_\lambda - \Delta\nu_T) \tag{2}$$

where the transitional frequency of the local oscillator ν_{Tj+n} is chosen so that $(f_\lambda - \Delta\nu_T)$ lies within the detector bandwidth.

CO_2 LASER FREQUENCY CHARACTERISTICS AND CONTROL

Local Oscillator Laser

For the specified transition wavelengths to oscillate in either laser, each laser must have a frequency tuning capability. Within a specified transition, the resonant frequency of a cavity mode is given by [17]

$$\nu_{mnq} = \nu_o \left\{ (q + 1) + \frac{1}{\pi} (m + n + 1) \cos^{-1} \sqrt{\left(1 - \frac{\ell}{R_1}\right)\left(1 - \frac{\ell}{R_2}\right)} \right\} \tag{3}$$

where the fundamental beat frequency is $\nu_o = c/2\ell$ for a cavity of length ℓ. Here q is the number of modes of the axial standing wave pattern, m and n are transverse mode numbers (rectangular coordinates), and R_1 and R_2 are the radii of curvatures of the laser mirrors. The long term stability must be within a fraction of the Doppler width. For low pressure lasers (below 10 torr), the gas is Doppler broadened and the line shape function is Gaussian centered at ν_T (molecular transitional line center frequency) with a line width given by [18]

$$\Delta\nu_{dop} = \frac{2\nu_T}{c} \sqrt{\frac{2kT \log 2}{m}} \tag{4}$$

where

$\Delta\nu_{dop}$ = Doppler broadened gainwidth at half maximum
c = velocity of light
k = Boltzmann's constant
T = absolute temperature
m = molecular mass.

Figure 4 illustrates the frequency selectivity process. The tunability of conventional CO_2 lasers is limited by the above formula to about ±60 MHz. [19] Hence a stability of less than several megahertz is required. Above 10 torr, collisional broadening of the molecular linewidth occurs at a rate between 4 and 5 MHz/torr. [20] A tunable range of 800 MHz has been reported by McElroy et al. [19]

The local oscillator laser can be constrained to oscillate on one transition (thereby eliminating mode hop-

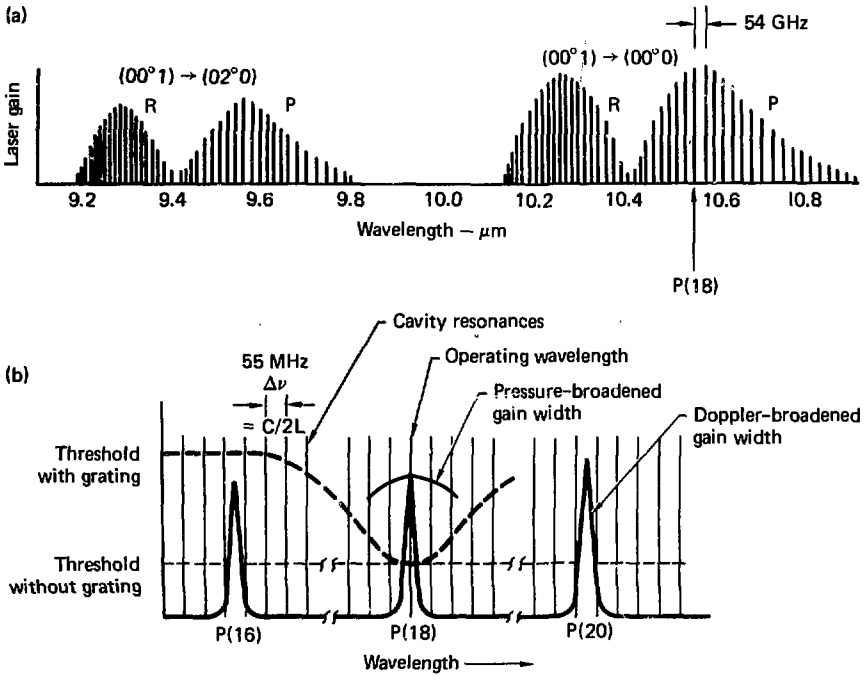

Fig. 4. CO_2 laser gain curves. (a) Unmodified gain and absorption spectra of wavelength control gases. (b) Gain vs wavelength for three lines of the spectra showing cavity resonances and threshold levels.

ping) through the use of a blazed grating, serving multiple functions as a laser mirror, line selector, and polarizer (dashed line in Fig. 4). As a mirror, the grating (e.g., ruled at 70 lines/mm, blaze angle 22°, $R_f = 20\,m$) is 97% reflective. As a polarizer, the grating is 80% efficient. By adjusting the angle of the grating, the laser can be made to oscillate on any of 16 separate transitions in the 00°1-10°0 branch. These transitions range in wavelength from 10.467 μm to 10.788 μm. Further, through the use of isotopes of carbon and oxygen, operation on 11.1, 11.7, or 9.4 μm bands is possible, yielding a total of 64 separate available wavelengths. A 50 mW minimum power output (more than sufficient for the heterodyne receiver described here) with the above attributes is commercially available.

Stark Cell Frequency Stabilization

When the desired transition is selected by the mirror grating, the local oscillator may be tuned over a frequency range of ±300 MHz or more by axially positioning the reflective mirror. This is accomplished by mounting the mirror on a piezoelectric bender. Stabilization is achieved by directing some of the source laser energy through the Stark cell and locking the laser frequency to the Stark absorption line.[21] A dc electrical field applied to the cell causes the frequency of the absorption line and, therefore, the laser frequency to be tuned. Long-term and short-term laser frequency stability of 100 kHz has been achieved. The important frequencies and bandwidths appear in Table I.

Table 1. Frequencies associated with infra-red scattering from MFTF plasma.

Source	Associated frequency
Fourier noise, 0.1 μsec risetime	10 MHz
Transverse electromagnetic (TEM) mode separation	12 MHz
Longitudinal mode separation for cavity of 268 cm	56 MHz
Frequency tuning stability for heterodyne system	<2 MHz (100 kHz achieved)
Doppler broadened (low pressure) gainwidth	60 MHz
Collisional broadened gainwidth, 200 torr Atmospheric	800 MHz 5 GHz
P-R convective instability in MFTF	500 MHz – 1 GHz
HgCdTe 3 dB bandwidth	1.2 GHz
Rotation-vibration line spacing	53.4 GHz
Bohm-Gross frequency for MFTF parameters and θ_s = 11 mrad	68 GHz
Fundamental 10.6 μm frequency	28.3 THz

HETERODYNE DETECTION WITH MERCURY CADMIUM TELLURIDE DETECTORS

Mercury cadmium telluride, $Hg_{1-x}Cd_xTe$, is an alloy semiconductor whose energy gap can be varied by changing the composition x of the alloy. [22,23] High-performance, intrinsic photovoltaic detectors with a spectral response between 8 μm and 14 μm have been developed. In particular, the Societe Anonyme des Telecommunications, Paris, has developed 10.6 μm liquid nitrogen-cooled photodiodes whose sensitive surface measures 0.2 mm × 0.2 mm. They possess a noise-equivalent power (NEP) of 8×10^{-20} W/Hz with a 1 mW local oscillator (Fig. 5), a 3dB cutoff of 1.2 GHz (Fig. 6), and a responsivity of 500 V/W.

In the case of coherent detection, the signal-to-noise (SNR) power ratio agrees with the expression [13]

$$(S/N)_{power} = \eta\, P_s/2\, h\nu\, \Delta f \qquad (5a)$$

where P_s is the signal power (scattered power at the detector), η the quantum efficiency of the detector, $h\nu$ is the photon energy (1.88×10^{-20} joules at 10.6 μm), and Δf is the receiver bandwidth. For a beam normally incident to the detector surface of Gaussian amplitude profile (TEM $_{00}$ mode), Eq. (5a) may be generalized to include geometrical efforts and is then given by [24]

$$(S/N)_{power} = (\eta\, I_s\, w^2/h\nu\, \Delta f)\, \exp(-\ell/4\, w^2)\, M\left(1, \frac{3}{2}, \frac{\ell^2}{8w^2}\right) \qquad (5b)$$

where I_s is the intensity in watts per unit area carried by a beam with a field half-width parameter w, [17] ℓ represents the dimension of an $\ell \times \ell$ detecting surface, and M is the confluent hypergeometric function. From Eq. (5b) the optimum detector-to-beam ratio is found to be $\ell/w = 2.7$. The SNR as given by Eq. (5a and b) for a quantum efficiency $\eta = 30\%$ is shown in Table 2 for the cases of coherent scattering from the ion-acoustic waves in Ref. 8 and the P-R instability in MFTF. Here, it is seen not only that large pulse powers yield a large SNR but also that a high power CW signal detected by a narrow bandwidth receiver can yield SNR's appreciably greater than unity. For parameters commonly associated with CW laser operation (useful in localizing waves or instabilities possessing a specific wavevector in the scattered spectrum and in system alignment), the SNR can be considerably below unity. However, an SNR of less than one can still be used. In photomixing, the output SNR is equal to the number of signal samples times the single sample input SNR. [25] A narrow

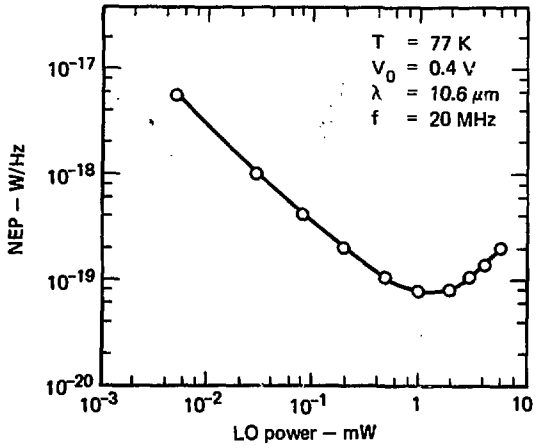

Fig. 5. Noise equivalent power data as a function of the local oscillator power obtained in heterodyne detection with HgCdTe PV cells.

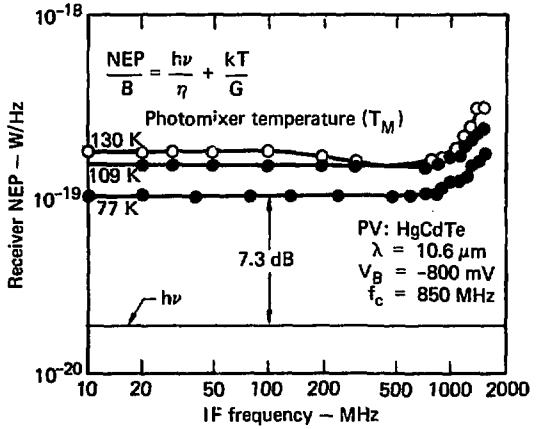

Fig. 6. Heterodyne receiver NEP versus intermediate frequency with temperature as a parameter.

band intermediate-frequency filter, with a bandwidth approximately equal to the reciprocal of the sample time, can serve as a post-detection integrator. For this purpose, lock-in amplifiers increase the level of the signal relative to noise by sampling (actually rectifying) the repetitive signal at a constant phase, and by relying upon noncoherent noise being rectified at random phase. However, for the CW scattering levels shown in Table 2, a typical lock-in amplifier acquisition time is 2 seconds at a 100 kHz reference frequency and, therefore, is beyond the lifetime of the MFTF plasma. Hence, detection of instability scattered power from a CW source should prove feasible only for relatively high-power CW lasers and narrower receiver bandwidths, provided the instability coherence length allows for Bragg scattering.

Table 2. Coherent scattering parameters for waves and instabilities.

Ion-Acoustic waves[8], $n_0 = 10^{11}$ cm^{-3}

P_s, W	Δf	f_λ	$\Delta f/f_\lambda$	ℓ_z cm	$\tilde{n}_e/n_0$	SNR	Comment
1.7×10^{-15}	300 kHz	5 MHz	6×10^{-2}	1	1.5×10^{-3}	0.0045	CW, low power, 1 W
1.7×10^{-15}	125 Hz*	5 MHz	2.5×10^{-5}	1	1.5×10^{-3}	100	CW, low power, *lock-in amplifier signal processor
1.13×10^{-10}	300 kHz	5 MHz	6×10^{-2}	1	1.5×10^{-3}	3000	Pulsed, high power
Post-Rosenbluth convective instability, $n_0 = 10^{14}$ cm^{-3}							
10^{-11}	100 MHz	1 GHz	10^{-1}	0.5	10^{-4}	0.8	CW, low power, 10 W
10^{-11}	10 MHz	1 GHz	10^{-3}	0.5	10^{-4}	80	CW, low power, 10 W
10^{-10}	30 MHz	1 GHz	3×10^{-2}	0.5	10^{-4}	27	CW, 100 W
1.5×10^{-7}	100 MHz	1 GHz	10^{-1}	0.5	10^{-4}	12,000	Pulsed, 150 kW

ALIGNMENT WITH EXTERNALLY EXCITED HIGH-FREQUENCY ACOUSTIC WAVES

The prior alignment of the light-mixing heterodyne detector optics is crucial to detecting and measuring waves and instabilities in plasma. As previously indicated, if the phase fronts of the incoming signal and local oscillator fields are not collinear, a rapid degradation of the signal output photocurrent can be expected. The alignment procedure consists of the following preparations:

1. Basic optical component positioning with 6328 Å HeNe light. For this to be done in normal room background light, a 10 mW minimum laser power output is required.
2. System tuning with CW CO_2 light. As the refractive indices of the lenses and windows are wavelength dependent, 10.6 μm light must be used to "tune" the optical components to this particular wavelength. Positioning is accomplished with photoluminescent detectors and an ultraviolet light source with normal background light. Some shading by means of dark curtains has proved helpful, however.
3. $\underline{k}$ space alignment. To determine and calibrate the Bragg scattering angle accurately, wire gratings, with perodicity in the range of the plasma waves to be measured, have proved invaluable.
4. Receiver calibration and fine tuning by means of high-frequency pressure waves.

Item 4 requires additional comment. To test the entire system (optics and electronics) with readily controllable waves in a convenient medium, we propose to generate 100 MHz to 1 GHz waves in an acousto-optical crystal (an optical phase grating) located near the scattering volume and aligned perpendicular to the beam. A likely material is Al_2O_3, a low-loss transparent dielectric that supports 0.11 mm waves when excited at 100 MHz.[26] This corresponds to a 5.5° Bragg scattering angle. A suitable transducer for fundamental mode operation in the 100 MHz to 1 GHz band would be a thin evaporated layer of cadmium sulphide.[27]

COHERENT SCATTERING FROM THE POST-ROSENBLUTH CONVECTIVE INSTABILITY

The source of the P-R convective loss cone instability [28,29] is the population inversion resulting from the absence of particles having low kinetic energies in a mirror machine. Not unlike the action of a MASER, the attempt of higher state particles to fill lower state vacancies initiates the growth of an instability which convects and exponentiates along the mirror magnetic field. It is the larger physical dimensions of MFTF (machine length $L \gg \rho_i$ ion gyroradius) which provide the environment necessary for a significant number of high-energy ions to be pushed back into the loss cone. It should be noted that this process was strongly suspected to have dominated the low-energy ("quiescent") runs in the 2XII experiments. [30] Because of the shorter scale length L/ρ_i in the higher energy 2XIIB plasma, the convective instability is not important.

The P-R instability is described by a propagating electrostatic wave with a wavelength perpendicular to $\underline{B}$ in the range 0.1 mm to a few millimeters ($\lambda_{De} < \lambda_\perp \ll \rho_i$, where λ_{De} is the electron Debye length); it possesses a frequency comparable to the ion plasma frequency: 500 MHz to 1 GHz in MFTF.

The light scattered intensity into a solid angle $d\Omega$ and bandwidth $\Delta\omega_s$ due to propagating plasma waves is given by [8]

$$P_s d\Omega \Delta\omega_s = P_i\, r_0^2\, \tilde{n}_e^2\, \ell_z^2\, \lambda_i^2\, d\underline{k}_\perp\, \delta(\underline{k}_\lambda - \Delta\underline{k}) \tag{6}$$

for $\Delta\omega = \omega_\lambda$ in which $\Delta\omega$ and $\Delta\underline{k}$ satisfy

$$\Delta\omega = \omega_s - \omega_i \qquad \Delta\underline{k} = \underline{k}_s - \underline{k}_i$$

Here the subscripts s, i, λ denote scattered, incident, and wave quantities. The wavevector $\underline{k}_i$ is determined by the direction of the incident laser beam, while $\underline{k}_s$ is experimentally chosen as the direction (opposite that) being viewed. Equation (6) predicts a nonzero scattered contribution only when

$$\underline{k}_\lambda = \Delta\underline{k} \cong 2\,|\underline{k}_i| \sin\Theta_B/2 \tag{7}$$

or equivalently,

$$\sin\frac{\Theta_B}{2} = \frac{\lambda_i}{2\lambda} \tag{8}$$

Equation (8) is simply the acoustic analog of Bragg's law at Bragg angle θ_B for an electromagnetic field of wavelength λ_i incident upon a propagating field of wavelength λ.

The instability/fluctuation amplitude $\tilde{n}_e$ in Eq. (5a and b) may be found from a relationship between $\tilde{n}_e$ and E, the instability electric field strength. The static form factor (power spectrum of density fluctuations in $\underline{k}$ space) of a many-particle system is [31]

$$S(\underline{k}) = \frac{1}{N}\left\langle |\delta\rho_K(t)|^2 \right\rangle \tag{9}$$

where N is the number of particles of charge q and mass m in a volume V. The parameter $\delta\rho_K(t)$ represents the spatial Fourier components of the density fluctuations, while the brackets denote an ensemble average. From an energy spectrum relationship, we have [32]

$$\left\langle |E^2|(\underline{k}) \right\rangle = \frac{16\pi^2 Ne^2}{k^2}\, S(\underline{k}) \tag{10}$$

for an undamped collective mode with wavenumber k. Hence, we find for a resonant oscillation (the instability)

$$\frac{\left\langle |\delta\rho_K(t)|^2 \right\rangle}{n^2} = \frac{k^2}{16\pi^2 e^2 n_o^2} \left\langle |E^2|(\underline{k}) \right\rangle = \frac{\lambda_{D_i}\, k^2}{4\pi P_i} \left\langle |E^2|(\underline{k}) \right\rangle \tag{11}$$

where λ_{Di} is the ion Debye length and $P_i = n_0 T_i$ is the ion kinetic pressure. Relating the Fokker-Planck coefficient [33]

$$D = \frac{q_i^2}{2m_i^2} \int_{-\infty}^{\infty} dt' \left\langle E(\underline{r},t)\, E(\underline{r}',t') \right\rangle \cong \frac{q_i^2}{m_i^2\, \omega_{pi}} \left\langle E^2 \right\rangle \tag{12}$$

to an expression given by Baldwin and Callen [34,35]

$$D \cong \frac{\bar{V}^2}{t_{drag}} \frac{e^A}{(1+\epsilon_e)^2} , \tag{13}$$

where

$$\bar{V}^2 = \frac{T_i}{m_i} ,$$

we obtain

$$\left\langle E^2 \right\rangle = \frac{4\pi\, P_i}{\omega_{pi}\, t_{drag}} \frac{e^A}{(1+\epsilon_e)^2} \tag{14}$$

where $t_{drag} = 1.4 \times 10^{12}\, T_e^{3/2}/n_0$ with T_e and n_0 in units of KeV and cm^{-3} respectively, ω_{pi} is the ion plasma frequency, and ϵ_e is the electronic portion of the warm plasma permittivity. The numerical factor A is

$$A \equiv 2 \int_{-L/2}^{L/2} ds\, I_m\, k_\parallel = \alpha \left(\frac{\omega_{p_e}/\omega_{c_e}}{\sqrt{1 + \omega_{p_e}^2/\omega_{c_e}^2}} \frac{L}{\rho_i} \right)_{\text{midplane}} , \tag{15}$$

$$\alpha \gtrsim 0.11 \Big/ \sqrt{R_m + 1}$$

for mirror ratio R_m in a machine of length L. Substituting Eq. (14) into Eq. (11) yields,

$$\frac{\left\langle |\delta\rho_K(t)|^2 \right\rangle}{n^2} = \frac{\lambda_{Di}^2\, k^2}{\omega_{p_i}\, t_{drag}} \frac{e^A}{(1+\epsilon_e)^2} . \tag{16}$$

In MFTF, where $R_m \sim 2$, $\epsilon_e \sim \omega_{p_e}^2/\omega_{c_e}^2 \sim 3$, $L/\rho_i \sim 100$, and $A \sim 5$ to 7, we obtain

$$\frac{\tilde{n}_e}{n_0} = \frac{\left\langle |\delta\rho_K(t)|^2 \right\rangle^{1/2}}{n} \sim 10^{-3} . \tag{17}$$

The expected coherently scattered power from P-R in MFTF is illustrated in Fig. 7. For a specified receiver bandwidth Δf, the heterodyne SNR dependency is shown in Fig. 8. These results have been used to calculate the source power/receiver bandwidth/SNR's appearing in Table 2 for a "worst case" amplitude $\tilde{n}_e/n_0 = 10^{-4}$.

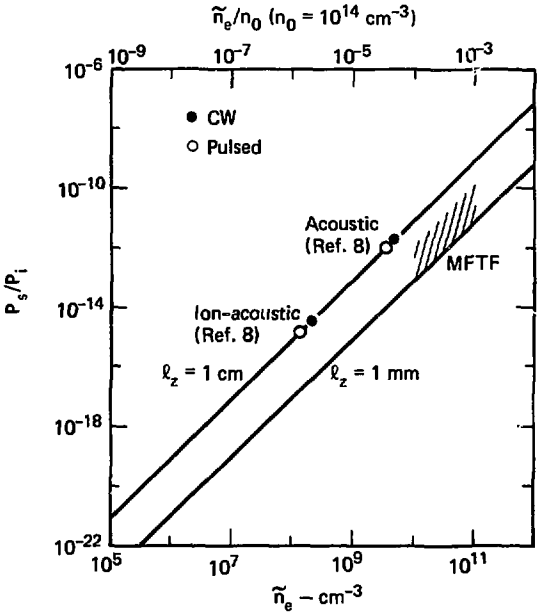

Fig. 7. Ratio of scattered to incident powers vs $\tilde{n}_e$ with Bragg distance ℓ_z as a parameter. Shown is Eq. (6) (solid lines), experimental pulsed laser data (open circles), and experimental CW laser data (closed circles).

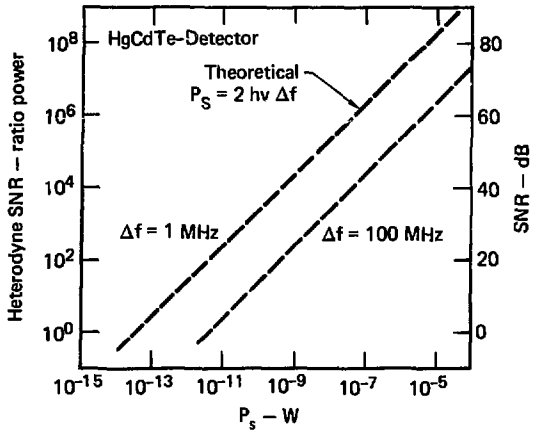

Fig. 8. Signal-to-noise ratio for HgCdTe detector at 10.6 μ in heterodyne mode of operation.

INCOHERENT SCATTERING FROM THERMAL FLUCTUATIONS

An incoherent scattering photon budget analysis is important, since incoherently received light can represent an appreciable percentage of the scattered power from background sources. Furthermore, if the coherence length of an instability under investigation is sufficiently short, the incoherent thermal spectrum represents a lower limit of the scattered power. In addition, at infrared frequencies the probing light wavelength in forward scattering experiments is long in comparison to fusion plasma Debye lengths. Hence the thermal Doppler-broadened spectrum as seen by the detector is correlated to internal natural plasma frequencies. This offers a possibility of directly measuring a number of plasma parameters that influence these correlations. This is in contrast to light scattering in the visible range from hot plasma where the thermal spectrum is uncorrelated, largely Gaussian in form and used to measure electron temperatures by Thomson scattering.

The thermal fluctuation scattered intensity into a solid angle $d\Omega$ and bandwidth $\Delta\omega_s$ is [8]

$$\left\langle [P_s \; d\Omega \Delta\omega_s] \right\rangle = P_i \; r_0^2 \; \lambda_i^2 \; n_0 \; \ell_z \int \frac{d\underline{k}_\perp}{(2\pi)^3} \int \frac{d\omega}{2\pi} \; S(\Delta\underline{k}, \; \Delta\omega) \tag{18}$$

where $S(\underline{k},\omega)$ is the spectral distribution factor for electron density fluctuations. [36] When operated in the high-power pulsed mode, the diagnostic system described here has the power and sensitivity to resolve the plasma thermal spectrum. For CO_2 laser light forward scattering the spectrum is correlated (the Salpeter parameter $\alpha = 1/k\lambda_D \approx 5$) with distinct ion and electron features as shown in Fig. 9 (a and b). For MFTF system parameters, Fig. 10 (a and b) shows that 21% of the incoherently scattered power appears in the ion feature, while 38% appears in a single wing of the electron feature located 68 GHz from the laser frequency (the Bohm-Gross frequency). The location of this line for a given plasma density and electron temperature is determined by the scattering angle θ_s. Thus by changing the angle of observation θ_s, this line may be set close to a vibrational line frequency (some multiple of 53.4 GHz) and measured when the heterodyne receiver option with a separate local oscillator laser is used. Table 3 delineates the fraction of total light scattered into a single 100 MHz wide frequency band at various locations of the spectrum, the scattered power as seen by the photocell mixer, and the power shot noise SNR expected for a 1 MW CO_2 system aligned to investigate both coherent (wave) and incoherent (thermal) scattering. Here, the solid angle Ω is 10^{-5} steradian. This is a small value for incoherent scattering and could easily be made a factor of 100 greater in the experimental situation, thereby improving the SNR (already above unity in the ion and electron features).

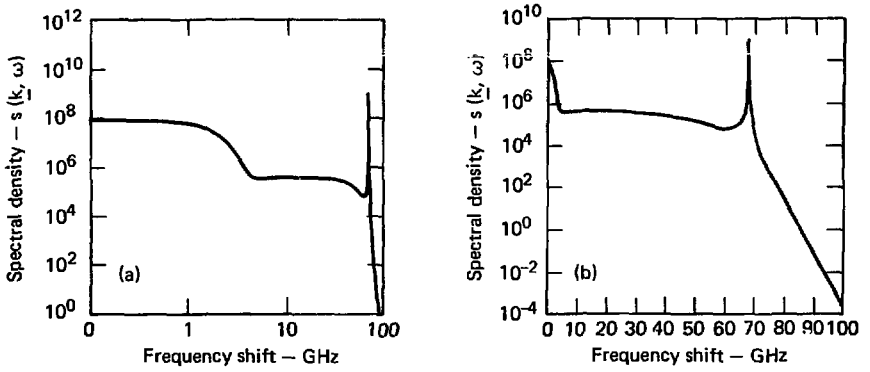

Fig. 9. Spectral density versus Doppler frequency shift for $\tilde{n}_e = 5 \times 10^{13}$ cm^{-3}, Te = 1 KeV, T_i = 30 KeV, θ_s = 11 mrad (α = 4.9) on logarithmic frequency (a) scale and on linear frequency scale (b).

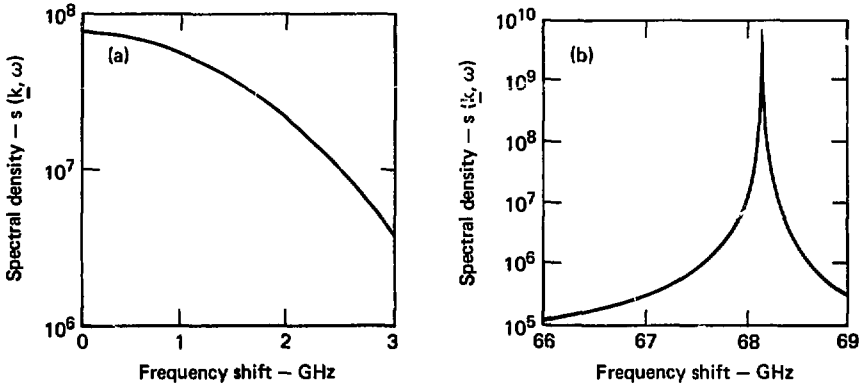

Fig. 10. Ion (a) and electron (b) features from Fig. 9.

Table 3. Incoherent scattering parameters for electron feature.[a]

Detector center frequency	Fraction of total light scattered	P_s at photocell (P_i = 1 MW)	SNR
68.14 GHz − 100 MHz	.0049	4.5×10^{-11} W	1.9
68.14 GHz	.3192	2.9×10^{-9} W	15
68.14 GHz + 100 MHz	.0481	4.4×10^{-10} W	6

[a]The numbers in the table are derived from the preceding equations based on the following parameters:

$n_0 = 5 \times 10^{13}$ cm^{-3}
$T_e = 1$ keV, $T_i = 30$ keV
$\Theta_s = 11$ mrad (0.6°)
$\alpha = 4.9$

Detection optics efficiency − 65%
Mixing efficiency − 70%
Detection bandwidth $\Delta f = 100$ MHz
Detection solid angle $d\Omega = 10^{-5}$ steradian

REFERENCES

1. M. Porkolab, *Physica*, **82C**, 86 (1976).
2. F. H. Coensgen, W. F. Cummins, A. W. Molvik, W. E. Nexsen, and T. C. Simonen, Fifth European Conference on Controlled Fusion and Plasma Physics (Euratom CEA, Grenoble, 1972), Vol. II, p. 71.
3. C. M. Surko, R. E. Slusher, D. R. Moler, and M. Porkolab, *Phys. Rev. Lett.*, **29**, 81 (1972).
4. R. E. Slusher, C. M. Surko, D. R. Moler, and M. Porkolab, *Phys. Rev. Lett.*, **36**, 674 (1976).
5. R. J. Goldston, E. Mazzucato, R. E. Slusher, and C. M. Surko, in Plasma Physics and Controlled Nuclear Fusion Research (Proc. 6th Int. Conf., Berchtesgaden, 1976), IAEA-CN-35/A-11 (IAEA, Vienna, 1977).
6. D. Masters and B. J. Rye, *Physics Letters*, **58A**, 108 (1976).
7. N. R. Heckenberg, "Single longitudinal mode operation of pulsed CO_2 lasers," Max-Planck Inst. für Plasmaphysik, Report IPP IV/83 (1975).
8. A. L. Peratt, R. L. Watterson, and H. Derfler, *Phys. Fluids*, **20** (1977).
9. A. Girard and A. J. Beaulieu, *IEEE J. Quant. Elect.*, **10**, 521 (1974).
10. A. E. Siegman, *Proc. IEEE*, **53**, 277 (1965).
11. H. Hirose and S. Kon, *Japan J. Appl. Phys.*, **16**, 533 (1977).
12. F. E. Goodwin and T. A. Nussmeier, IEEE *J. Quantum Elect*, **4**, 612 (1968); D. A. Kleinman and G. D. Boyd, *J. Appl. Phys.*, **40**, 546 (1969); H. W. Mocker, *App. Optics*, **8**, 677 (1969); B. Peyton, E. Sard, R. Lange, F. R. Arams, Proc. IEEE, **58**, 1769 (1970); B. J. Peyton, A. J. Dinardo, G. M. Kanischak, F. R. Arams, R. A. Lange, E. W. Sard, IEEE *J. Quant. Elect.*, **8**, 252 (1972).
13. M. C. Teich, *Coherent Detection in the Infrared*, in *Semiconductors and Semimetals*, edited by R. K. Willardson and A. C. Beer (Academic, New York, 1970), Chap. 9.
14. A. J. Forrester, R. A. Gudmundsen, and P. O. Johnson, *Phys. Rev.*, **99**, 1691 (1955).
15. R. W. Dixon and E. I. Gordon, *Bell Syst. Tech J.*, **46**, 367 (1967).
16. S. C. Cohen, *Appl. Optics*, **14**, 1953 (1975).
17. H. Kogelnik and T. Li, *Proc. IEEE*, **54**, 1312 (1966).
18. R. E. Jensen and M. S. Tobin, *IEEE J. Quant. Elect.*, **8**, 34 (1972).
19. J. H. McElroy, N. McAvoy, E. H. Johnson, J. J. Degnan, F. E. Goodwin, D. M. Henderson, T. A. Nussmeier, L. S. Stokes, B. J. Peyton, T. Flattan, *Proc. IEEE*, **65**, 221 (1977).
20. E. T. Gerry and D. A. Leonary, *Appl. Phys. Lett.*, **8**, 227 (1966).
21. T. A. Nussmeier and R. L. Abrams, *Appl. Phys. Lett.*, **25**, 615 (1974).
22. C. Vérie and M. Sirieix, *IEEE J. Quant. Elect.*, **8**, 180 (1972).
23. J. Marine and C. Motte, *Appl. Phys. Lett.*, **23**, 450 (1973).
24. L. Mandel and E. Wolf, *Journ. Opt. Soc. of America*, **65**, 413 (1975).
25. M. Ross, *Laser Receivers* (John Wiley and Sons, Inc., New York, 1966), p. 346.
26. D. A. Pinnow, *IEEE J. Quant. Elect.*, **6**, 223 (1970).
27. N. F. Foster, *Proc. IEEE*, **53**, 1400 (1965).
28. R. F. Post and M. N. Rosenbluth, *Phys. Fluids*, **9**, 730 (1966).
29. S. Ichimaru, *Basic Principles of Plasma Physics*, (W. A. Benjamin, Inc., Reading, Mass., 1973) p. 150.
30. F. H. Coensgen, Lawrence Livermore Laboratory, Livermore, Calif., MFTF Proposal LLL-Prop-142 (1976).
31. S. Ichimaru, op. cit., p. 193.
32. S. Ichimaru, op. cit., p. 219.
33. D. E. Baldwin, *Phys. Fluids*, **18**, 656 (1975).
34. D. E. Baldwin and J. D. Callen, *Phys. Rev. Lett.*, **28**, 1686 (1972).
35. F. H. Coensgen, op. cit., p. B-21.
36. A. L. Peratt, *Phys. Fluids*, **18**, 57 (1975).

CH/kjm/vt/cm